JACS
JOURNAL OF THE AMERICAN CHEMICAL SOCIETY

Article

pubs.acs.org/JACS

# Three-Dimensionally Homoconjugated Carbon-Bridged Oligophenylenevinylene for Perovskite Solar Cells

Qifan Yan,[†] Yunlong Guo,* Anna Ichimura, Hayato Tsuji,*[,‡] and Eiichi Nakamura*

Department of Chemistry, The University of Tokyo, 7-3-1 Hongo, Bunkyo-ku, Tokyo 113-0033, Japan

Supporting Information

**ABSTRACT:** Stabilization of the radical cationic state of a donor molecule by 3-D homoconjugation was probed using a substituted carbon-bridged oligophenylenevinylene backbone (COPV, or 5,5-diarylindeno[2,1-*a*]indenes). For molecules bearing electron-donating groups as the 5,5-aryl moieties, a one-electron oxidation of the COPV backbone results in delocalization of the cationic charge over the whole molecule with a small reorganization energy. The compounds forming a stable radical cation by 3-D homoconjugation produce a uniform amorphous film and show high short-circuit current, high fill factor, and hence high power-conversion efficiency when used as a hole-transporting layer of an organic−inorganic hybrid lead perovskite solar cell. This material thus shows a performance and stability in air comparable to those obtained with the benchmark material, **spiro-MeOTAD**.

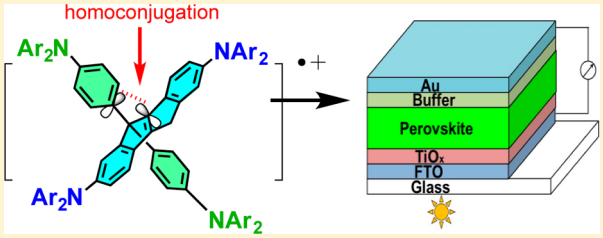


## INTRODUCTION

Stabilization of negative charge on a 3-D $\pi$-scaffold has attracted considerable attention from chemists since the discovery of the utility of fullerenes as electron-accepting material in organic and perovskite solar cells (SCs). Such 3-D molecules used as carrier-transporting materials tend to have a small reorganization energy and to give amorphous morphology suitable for carrier transport in a film. On the other hand, there has been a paucity of studies on the potential of 3-D stabilization of positive charge for hole transportation where, chemically speaking, a radical cation of hole-transporting material plays the role. Having found[1] that a carbon-bridged oligophenylenevinylene backbone (COPV, or 5,5-diaryl-indeno[2,1-*a*]indenes, **1**) provides a structurally robust 2-D $\pi$-scaffold (cyan, Figure 1a), we were intrigued by the possibility of 3-D homoconjugative stabilization of a radical cation through installation of additional electron-donating aminophenyl groups orthogonal to the plane of the COPV $\pi$-system (Figure 1a). We report here the synthesis, properties, and SC application of the new electron-rich $\pi$-system (**1**−**3**, Figure 1b) examined for the effects of the 3-D homoconjugative stabilization of a radical cationic state. The compounds form an effective, amorphous hole-transporting layer (HTL) for a thin-film semitransparent[2] lead perovskite SC device,[3] which are already finding use in "solar window" applications.[4] The perovskite SCs using **1**−**3** show a level of power-conversion efficiency (PCE) and stability in air comparable to those with the popularly employed **spiro-MeOTAD** (Figure 1b, bottom)—a benchmark of hole-transporting material.[5] Reference compounds **4**−**6**, which have only the flat 2-D conjugated system, were found to perform poorly as an HTL in spite of the similarity of their oxidation potentials to those of **1**−**3**. Compounds **1**−**3** form a stable radical cation and produce a uniform amorphous film; thus, they showed high short-circuit current ($J_{sc}$), high fill factor (FF), and hence high PCE. Compound **4**, which forms an amorphous film but is incapable of homoconjugative stabilization of a radical cation, showed high $J_{sc}$ but poor FF. Compounds **5** and **6**, which form a crystalline film and are incapable of radical cation stabilization, showed poor performance for $J_{sc}$, open-circuit voltage ($V_{oc}$), FF, and PCE. A simple fluorene **7**, lacking the ability of stabilizing its oxidized form, showed a low performance and poor stability in air.

## RESULTS AND DISCUSSION

**Synthesis of COPVs 1−5.** The flat 2-D $\pi$-system of COPVs has been found to be useful for dye-sensitized SCs,[6] solid-state organic lasers,[7] molecular wires,[8] and energy and electron donors.[9] COPV has a 2-D conjugated system flanked by geminal substituents (e.g., at C5) that forms a 3-D scaffold, preventing intermolecular interactions. To study the feasibility of creating a 3-D homoconjugated donor system,[9] we installed four (4-arylamino)phenyl donor groups on both ends of the COPV skeleton and on one of the geminal diphenyl groups (at C5) as in **1**−**3**, expecting that the COPV system and the geminal C5 groups would become homoconjugated in the radical cationic state. Compound **3** has a spiro-linkage mimicking **spiro-MeOTAD**, **2** is an open-chain analogue of **3**, and **1** is its 4-aminophenyl isomer. For comparison, we also synthesized bis(4-diarylamino)phenyl COPVs **4**−**6**, lacking the electron-donating geminal groups (Scheme 1).

**Physical and Optical Properties of COPV.** In the neutral state of **1**−**3**, there was little sign of interaction between the

**Received:** April 19, 2016
**Published:** August 5, 2016

  

DOI: 10.1021/jacs.6b04002
J. Am. Chem. Soc. 2016, 138, 10897−10904

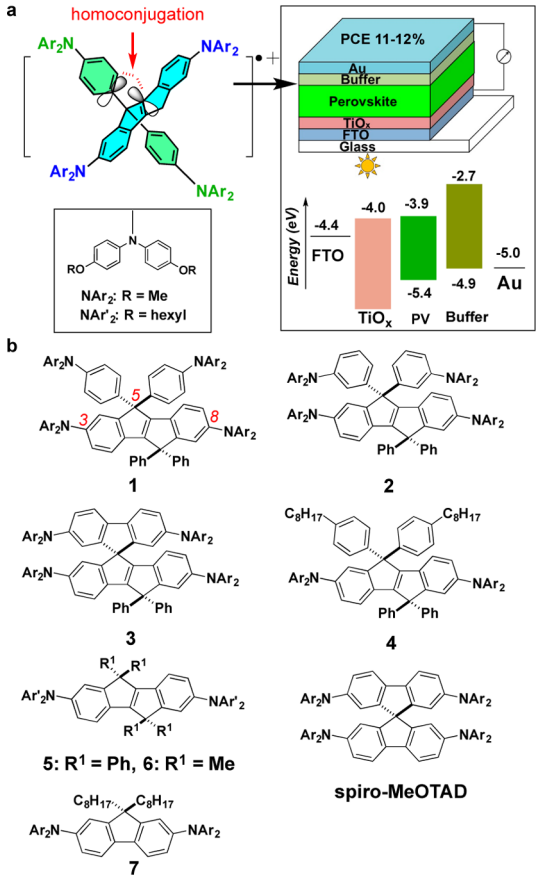


**Figure 1.** SC device configuration and molecular structures in our study. (a) Schematic illustration of three-dimensional homoconjugation in COPV **1** and SC device configuration as well as energy diagram. (b) Structures of COPVs **1**–**6** (numbering of carbon atoms on COPV is indicated in italic red numbers) and reference molecules **spiro-MeOTAD** and **7**.

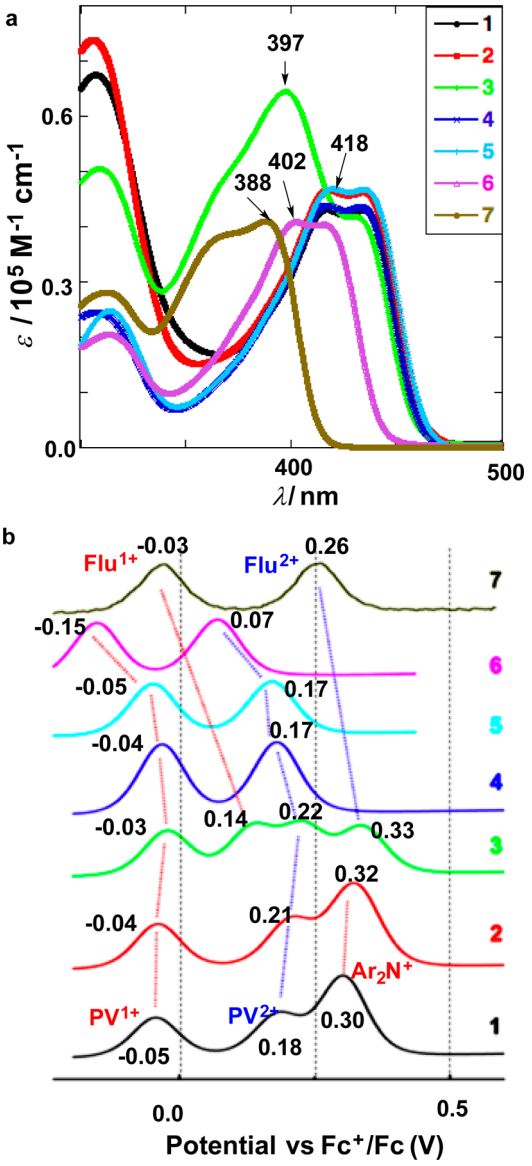


**Figure 2.** Photo- and electrochemical properties of **1**–**7**. (a) UV–vis absorption spectra of compounds **1**–**7** in dilute PhCl solutions at 5 $\mu$M. (b) Differential pulse voltammetry (bottom) of compounds **1**–**7** in *ortho*-dichlorobenzene/$CH_3CN$ (v/v, 4/1) at 0.5 mM. Oxidative peaks are labeled with the species primarily involved in the oxidation. Abbreviations: PV, bisdiarylamino COPV moiety; Flu, bisdiarylaminofluorene moiety; $Ar_2N$, diarylamino moiety on the C5 positions in **1** and **2**. Broken lines show peak correlation.

**Scheme 1. Synthesis of COPVs 1–5**

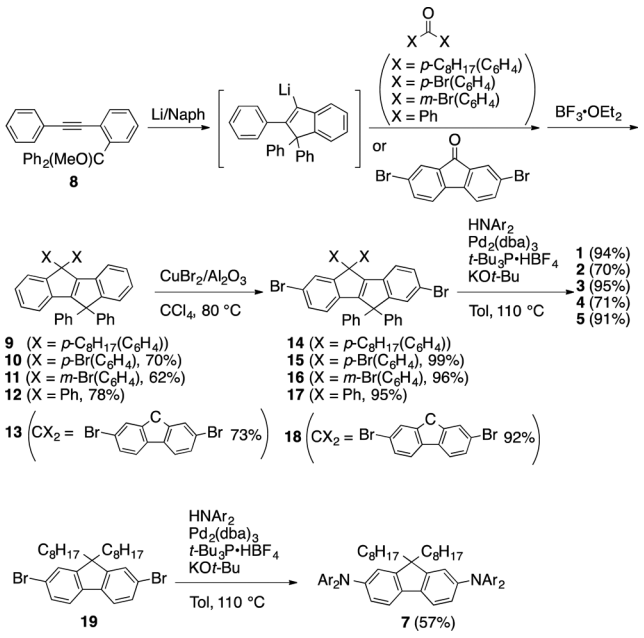


amino COPV and the geminal 4-aminophenyl groups. For example, **1**–**3** (Figure 2a) show an absorption band centered at 420 nm due to a $\pi$–$\pi^*$ electronic transition of the COPV framework, identical to that of **4** and **5**. However, **3** shows an additional band at 397 nm due to a $\pi$–$\pi^*$ electronic transition at the fluorene moiety. In addition, **1**–**5** all emit at 463–470 nm upon photoexcitation, with almost identical fluorescence quantum yield and lifetime (Table 1), suggesting that photoexcitation of **1**–**5** involves almost solely the COPV system.

Then, a strong interaction between the radical cation of the COPV moiety and the electron-rich geminal groups was identified by differential pulse voltammetry (DPV; Figure 2b). The electrochemical data in Figure 2b provide evidence for strong interaction between the COPV framework and the electron-rich geminal groups in the radical cation state of **1**–**3**,



DOI: 10.1021/jacs.6b04002
J. Am. Chem. Soc. 2016, 138, 10897–10904

Table 1. Photophysical and Electrochemical Data[a]

| compd | $\lambda_{abs}$/nm | $\varepsilon/10^4$ $M^{-1}$ $cm^{-1}$ | $\lambda_{fl}$/ nm | $\Phi_{fl}$ | $\tau$/ns | $E_{ox}$/V |
|---|---|---|---|---|---|---|
| 1 | 417/435 | 4.3/4.3 | 465 | 0.87 | 2.03 | −0.05, 0.18, 0.30 (2e) |
| 2 | 418/435 | 4.7/4.6 | 467 | 0.91 | 2.06 | −0.04, 0.21, 0.32 (2e) |
| 3 | 397/431 | 6.4/4.2 | 463 | 0.87 | 2.02 | −0.03, 0.14, 0.22, 0.33 |
| 4 | 417/433 | 4.4/4.4 | 466 | 0.83 | 1.86 | −0.04, 0.17 |
| 5 | 420/435 | 4.7/4.7 | 470 | 0.80 | 1.93 | −0.05, 0.17 |
| 6 | 402/416 | 4.1/4.0 | 447 | 0.84 | 1.53 | −0.15, 0.07 |
| 7 | 388 | 3.5 | 417 | 0.50 | 1.27 | −0.03, 0.26 |

[a]$\Phi_{fl}$ (fluorescence quantum yield) was determined using an absolute method; $\tau$ (fluorescence lifetime) was measured using a time-correlated single-photon counting method with a 405 nm NanoLED for **1**−**6** and a 365 nm NanoLED for **7**, as excitation source and fitted single-exponentially with $\chi^2$ = 0.89−1.21; $E_{ox}$ was calculated against $Fc^+$/Fc couple as external reference.

but not that of **4** and **5**. The fluorene reference compound **7** shows the first and second oxidation peaks ($Flu^+$, $Flu^{2+}$; Figure 2 top) at −0.03 and 0.26 V (vs $Fc^+$/Fc couple), respectively. The amino COPV reference compounds **4** and **5** show the corresponding peaks ($PV^+$, $PV^{2+}$) at −0.04/0.17 V and −0.05/0.17 V, respectively, and the tetramethyl analogue COPV **6** (−0.15/0.07 V) is slightly easier to oxidize. It is notable that the diaminofluorene COPV **3** shows the $Flu^+$ and $Flu^{2+}$ peaks at 0.14 and 0.33 V, much higher by 0.17 and 0.07 V than those of the fluorene reference **7**, indicating that the oxidation of the fluorene moiety becomes much more difficult once the COPV moiety is oxidized ($PV^+$). Likewise, oxidation of the 4-aminoaryl groups in **1** and **2** becomes so difficult that they are oxidized only after the second oxidation of the COPV core ($PV^{2+}$).

**Characteristics of Neutral and Radical Cation.** Absorption titration experiments on chemical oxidation provided further support for the homoconjugation between the radical cation of the COPV moiety and the 4-aminophenyl group in **3**. Thus, a solution of compounds **3**, **4**, and **7** in chlorobenzene was treated with aliquots of nitrosonium hexafluorophosphate ($NO^+PF_6^-$), monitored with UV−vis absorption (Figure 3 and Figure S1). Upon addition of the oxidant to a solution of the aminofluorene **7**, a new peak at 522 nm rose at the expense of the band at 397 nm of the neutral molecule (Figure 3a). The 522 nm peak is due to the SOMO-to-LUMO transition of the fluorene radical cation. Similarly to the previously reported parent COPV **1**,[1a] the radical cation of **4** shows absorptions at 665 and 616 nm due to 0−0 and 0−1 transitions, respectively (Figure 3b). In **3** (Figure 3c), where fluorene and indeno[2,1-*a*]indene moieties are homoconjugated, the three bands developed simultaneously, indicating that both the COPV and the geminal 4-aminophenyl groups contribute to this spectral change because of formation of the radical cation (see SI for full range UV−vis−NIR spectra of **1**−**5** upon oxidation).

Density functional theory (DFT) calculations on both neutral and radical cation states of COPV **1**−**6** were carried out at the B3LYP/6-31G(d,p) theory level (details in Supporting Information (SI), Figures S2−S7). The calculated total positive charge on the two aminophenyl groups in the radical cations of **1**, **2**, and **3** are 0.27, 0.20, and 0.34, respectively, whereas that of **4** was only 0.08. Similarly, the spin

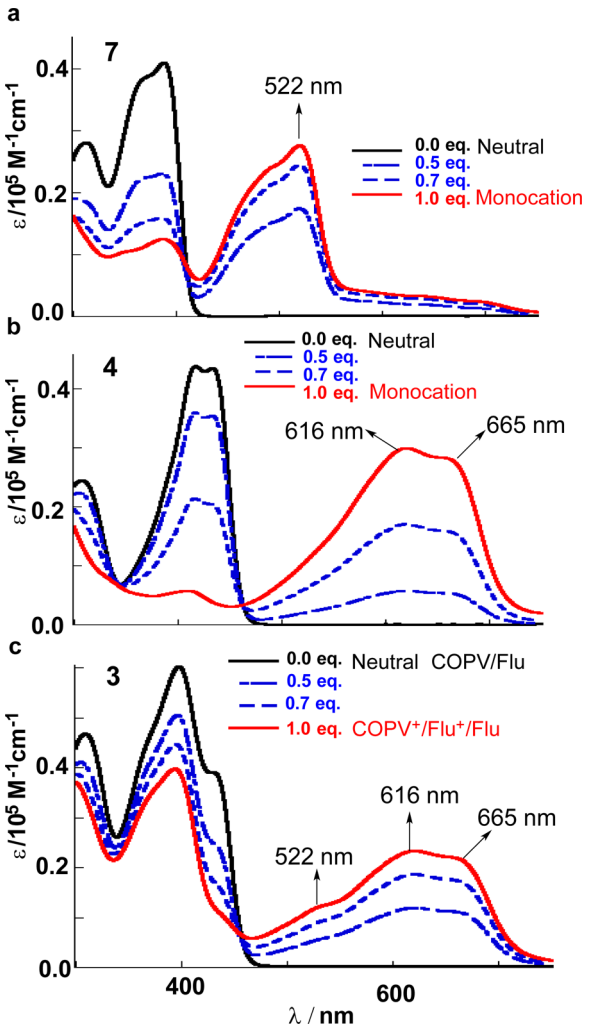


**Figure 3.** Titration experiments monitored by UV−vis absorption spectra of a solution in PhCl at 5 $\mu$M upon addition of $NO^+PF_6^-$: (a) **7**, (b) **4**, and (c) **3**. Arrows indicate local maxima.

density of the radical cation of **3** delocalizes significantly on the fluorene part, as shown in Figure S8. This is in stark contrast to compound **4**; the spin density of $\mathbf{4}^{\bullet+}$ resided mainly on the COPV moiety (see SI for HOMOs of the neutral compounds).

Careful comparison of the charge distribution between neutral and radical cation and the geometry parameters supports the existence of homoconjugation in the radical cation (Table 2). For example, the reorganization energies upon formation of the radical cations for **3** were clearly smaller than those for **4**−**6** (Table 2, second column). Upon removal of one electron from COPV **1**−**5**, the distance *l* shown by a red arrow in Figure 4a shortens most significantly for **1** and **3**. In agreement with this structural change, the radical cations of **1** and **3** showed a larger positive charge on the geminal aryl groups. The compounds **4** and **5** lack electron-donating diamine groups on the phenyl groups, and hence the phenyl groups cannot take part in homoconjugation when the compounds are oxidized (see Figure 2b, DPV). Smaller homoconjugation in **4**−**6** is seen in the smaller values of the positive change and the distance reduction in Table 2.

The ESR spectra of **1**−**4** in solution verified the radical nature of the oxidized species (Figure 4b). The radical cation of reference **4** showed an ESR signal with a *g* value of 2.00040, which is typical for organic radicals. Radical cations of **1**−**3** also


DOI: 10.1021/jacs.6b04002
J. Am. Chem. Soc. 2016, 138, 10897−10904

**Table 2. DFT Analysis of Radical Cations of 1−6 at the B3LYP/6-31G(d,p) Level of Theory**[a]

| compd | charge on C5 substituents | reorganization energy/eV | distance reduction/Å (%) |
|---|---|---|---|
| **1** | 0.27 | 0.28 | 0.015 (0.60%) |
| **2** | 0.20 | 0.27 | 0.003 (0.13%) |
| **3** | 0.34 | 0.21 | 0.009 (0.36%) |
| **4** | 0.08 | 0.25 | 0.004 (0.17%) |
| **5** | 0.07 | 0.25 | 0.004 (0.14%) |
| **6** | 0.06 | 0.29 | 0.001 (0.04%) |

[a]The charge on the C5 substituents refers to the difference between the neutral and radical cationic states. Distance reduction refers to the shortening of the distance between the *ipso*-phenyl carbon atom bonded to C5 and the vinyl carbon bonded to C5, as indicated by a red arrow in Figure 4a.

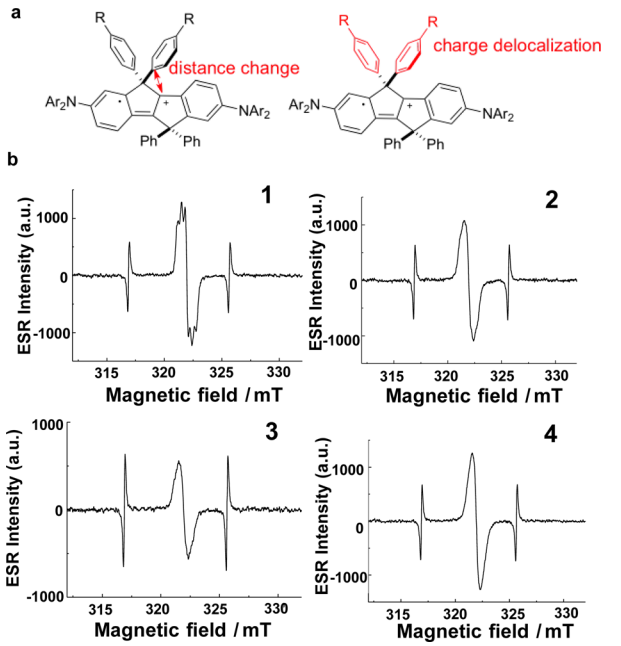


**Figure 4.** Properties of radical cations. (a) Illustration of the carbon−carbon distance and charge delocalization in the radical cation. (b) ESR spectra of the radical cations of **1**−**4** in PhCl.

exhibited similar *g* values of 2.00039, 2.00038, and 2.00046, respectively. It is notable that the ESR spectrum of the radical cation of **1** displayed pronounced hyperfine structure caused by intervalence charge transfer with diaryl amino groups on C5,implying effective interactions between the COPV moiety and substituents in $\mathbf{1}^{\bullet+}$.[10a] Broadened ESR signal were observed for $\mathbf{2}^{\bullet+}$ and $\mathbf{3}^{\bullet+}$, suggesting delocalized radical. In comparison, ESR spectrum of $\mathbf{4}^{\bullet+}$ displayed a much sharper peak without hyperfine structure, indicative of a less delocalized radical (Figure 4b).[10b] These results further suggest that the homoconjugation is much more pronounced in the radical cations of **1**−**3** than that of **4**.

**Solar Cells Based on COPV as Hole-Transporting Layer.** The above studies indicate COPVs' potential usefulness as HTL materials, if the orbital energy levels match with the potentials of PV and Au electrode. It was indeed the case. By photoemission yield spectroscopy, we determined the HOMO level of all of the compounds in their film state to be −4.9 eV (−4.8 eV for **6**). From the onset of the UV−vis absorption spectra, we determined the band gap (Table S7 and Figure 2a). These data suggest that they are suitable for blocking electrons and transporting holes.

Measurements of hole mobility and conductivity for doped and undoped compounds **1**−**7** as well as **spiro-MeOTAD** indicated that doping of our compounds slightly increases the mobility and the conductivity, and the data for the doped compound are comparable to those of **spiro-MeOTAD** (in the order of $10^{-5}$ $cm^2$ $V^{-1}$ $s^{-1}$ and $10^{-6}$ S/cm, respectively). These data obtained for ITO/PEDOT:PSS/HTL(or HTL-doped)/Au are shown in Figures S9 and S10 and Table S8.

Encouraged by the theoretical and experimental data suggesting good hole-transporting ability of a film of COPV **1**−**3**, we examined their potential as a buffer layer in thin-film perovskite SC devices, using **4**−**7** as references. For this purpose we employed a planar $TiO_x$ as an ETL in our test semitransparent SC devices, which we could reproducibly fabricate in our hand. A solution of the COPVs and dopants, lithium bis(trifluoromethanesulfonyl)imide (Li-TFSI) and 2,6-di-*tert*-butylpyridine (TBP), was spin-coated on a lead perovskite layer prepared as reported previously.[11] The whole SC device consists of FTO/$TiO_x$ (45 nm)/$CH_3NH_3PbI_{3-x}Cl_x$ (230 nm)/buffer layer (200 nm)/Au (80 nm)/CYTOP and tested under AM 1.5G illumination with a power density of 100 mW $cm^{-2}$. This device shows an average transparency of ca. 25% without metal electrode.

As shown in Figure 5a, the device consists of very uniform layers of perovskite and doped compound **1** as imaged with a

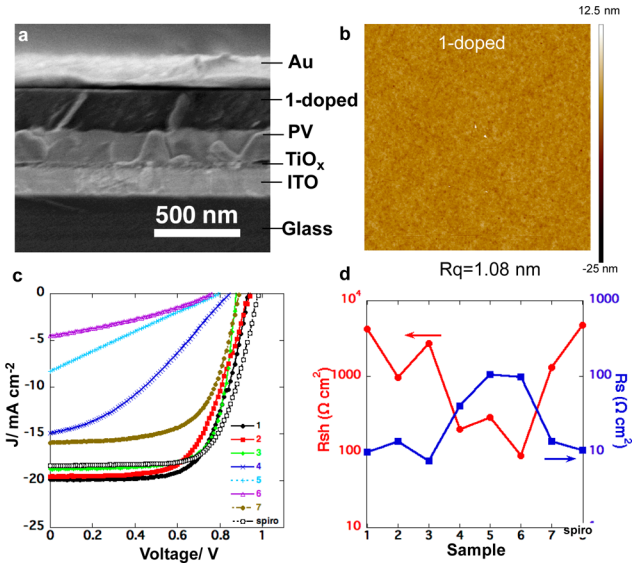


**Figure 5.** Cross-section image of SC, surface morphology of doped compound **1** and *J*−*V* characteristics of SC devices under AM 1.5G illumination. (a) Cross-section SEM image of device. Perovskite, TiOx, and ITO layers containing heavy metals are seen as gray layers because they emit more backscattered electrons than organic materials, and hence the organic HTL is seen to be darker. (b) AFM image of doped compound **1**. (c) *J*−*V* curves. (d) Relationships between different SCs and shunt resistance, $R_{sh}$, as well as series resistance, $R_s$.

low landing voltage scanning electron microscopy (SEM). Such SEM allows us to image directly the surface of conducting and insulating materials without metal coating that is usually required for conventional SEM imaging (to avoid sample charging).

As shown in the bottom of Table 3, the reference perovskite SC system, studied here for a popular buffer, **spiro-MeOTAD**,


DOI: 10.1021/jacs.6b04002
J. Am. Chem. Soc. 2016, 138, 10897−10904

**Table 3. Performance Parameters of Thin-Film Perovskite SCs Using Different Buffer Layers (See Text for Details)**

| compd | $J_{sc}$/ mA cm$^{-2}$ | $V_{oc}$/V | FF | PCE/% | $R_{sh}$/ kΩ cm$^2$ | $R_s$/ Ω cm$^2$ |
|---|---|---|---|---|---|---|
| **1** | 19.9 | 0.93 | 0.66 | 12.3 | 4.26 | 10.1 |
| **2** | 19.6 | 0.94 | 0.61 | 11.2 | 0.97 | 13.8 |
| **3** | 18.7 | 0.88 | 0.73 | 12.0 | 2.70 | 7.7 |
| **4** | 14.9 | 0.85 | 0.35 | 4.4 | 0.20 | 40.5 |
| **5**[a] | 4.5 | 0.76 | 0.33 | 1.1 | 0.29 | 106 |
| **6** | 8.3 | 0.80 | 0.24 | 1.6 | 0.09 | 98 |
| **7** | 15.9 | 0.89 | 0.63 | 8.9 | 1.30 | 14.0 |
| **spiro-MeOTAD** | 18.4 | 0.98 | 0.68 | 12.2 | 4.76 | 10.6 |

[a]Doped with FK209. $R_{sh}$ and $R_s$ obtained from the $J-V$ curve in Figure 5.

shows a PCE of 12.2% with $J_{sc}$ = 18.4 mA cm$^{-2}$, $V_{oc}$ = 0.98 V, and FF = 0.68, as shown in the bottom of Table 3, and the efficacies of the homoconjugated compounds **1**–**3** were found to be comparable. For example, a **1**-based device showed a PCE of 12.3% with $J_{sc}$ = 19.9 mA cm$^{-2}$, $V_{oc}$ = 0.93 V, and FF = 0.66. The highest performance of **1** coincides well with the highest degree of homoconjugation in the radical cationic state as discussed above.

COPVs **1**–**4** behave similarly in terms of the amorphous nature of the films, as shown by the lack of XRD peaks and by absorption spectra almost identical to those in solution (Figures S11 and S12). Therefore, we expect a smooth interface with perovskite and hence a high ability of the film to collect charge at the interface with the perovskite film. In Figure 5b and Figure S13 is shown the very smooth surface of HTL of doped compound **1** (root-mean-square roughness ($R_q$) of 1.08 nm) as studied by atomic-force microscopy (AFM). This is supported by the high $J_{sc}$ values of 14.9–19.9 mA cm$^{-2}$ for **1**–**4** (Table 3). However, reference **4** differs markedly from **1**–**3** for its very small FF = 0.35, large $R_s$ = 40.5 Ω cm$^2$, and PCE of 4.4%, indicative of poor hole-conducting ability in our device. A device using the fluorene reference compound **7** showed PCE of 8.9% (best data among multiple runs), which is 26% lower than a **spiro-MeOTAD** device. Meanwhile, the stability of SC using compound **7** was much worse than other HTLs: The PCE value decreased to 20% of original value after 48 h in air (Figure 6a) accompanying the color the PV film (Figure 6b). Note that the stability of the devices was found to be comparable using compound **1** and **spiro-MeOTAD**. We can ascribe these to the lack of homoconjugative stabilization of the radical cation, which plays a key role in the increase of the device stability and the hole-transporting ability of HTL.

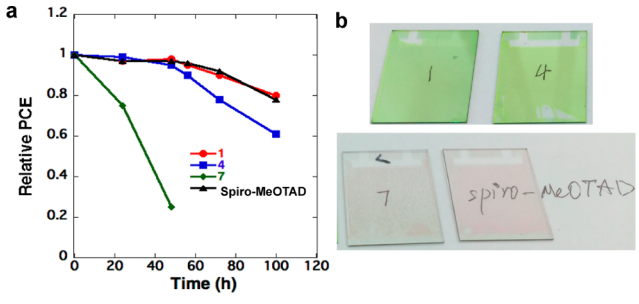


**Figure 6.** Stability of the solar cells using various HTL materials. (a) Relative PCE of solar cells based on different HTLs. (b) Appearance of various devices after 48 h in air with humidity about 40%.

In contrast to **1**–**4**, **5** and **6** form a crystalline film, as shown by the appearance of XRD diffraction peaks (**5**, $2\theta$ = 3.47°, $d$ = 2.54 nm; **6**, $2\theta$ = 6.33°, $d$ = 1.39 nm; see Figure S11), which would cause poor contact with the perovskite layer and insufficient charge collection. Therefore, we found a small $R_{sh}$, large $R_s$, and very small $J_{sc}$ of 4.5 and 8.3 mA cm$^{-2}$ for **5** and **6**, respectively (Table 3).

## CONCLUSION

In summary, we have probed the origin of the high hole-transporting ability of popular **spiro-MeOTAD** and found that stabilization of a radical cationic state through 3-D homoconjugation can serve as a generally useful strategy for the design of an amorphous and efficient HTL in a perovskite SC. A few key features of the 3-D COPV system have been identified to be critical for good performance. First, the 3-D homoconjugated system has intrinsically smaller reorganization energy than the flat 2-D system and hence contributes to higher charge transporting ability. Second, the multiply substituted system allows tuning of the energy levels of HOMO and LUMO of the film through structural changes of the donor groups to obtain maximum hole conductivity. We envisage that longer COPV systems will provide further electronic tuning.[7] Third, a 3-D system tends to form an amorphous film and hence produces a smoother interface with neighboring layers to increase the current density. The high performance of **1**, comparable with that of **spiro-MeOTAD**, supports the importance of 3-D homoconjugation.[12] Overall, the homoconjugation strategy based on the COPV skeleton improves charge carrier transportation without affecting the energy levels of the HOMO and LUMO of the HTL and hence is useful for the control of carrier injection. Taking our findings combined with recent information on the PV formation mechanism,[13] we can now have a prospect for designing PV devices through rational chemical design of the active layer and interlayers.

## EXPERIMENTAL SECTION

**General Information for Synthetic Procedures.** All oxygen- and moisture-sensitive reactions were performed under a nitrogen atmosphere using the standard Schlenk method, lithium/naphthalene reagent was prepared under an argon atmosphere. Analytical thin-layer chromatography (TLC) was performed using glass plates precoated with 0.25 mm, 230–400 mesh silica gel impregnated with a fluorescent indicator (254 nm). TLC plates were visualized by exposure to ultraviolet (UV) light. Flash column chromatography was performed on Kanto silica gel 60 (spherical, neutral, 140–325 mesh).[14] Chemicals were purchased from Tokyo Kasei Co. and Aldrich Inc., and used as received unless otherwise indicated. Reagent grade tetrahydrofuran (THF) and toluene (Tol) were purified using a solvent-purification system. The following compounds were prepared following the literature: bis(4-octylphenyl)methanone,[15] bis(4-bromophenyl)methanone,[16] bis(3-bromophenyl)methanone,[17] and $CuBr_2/Al_2O_3$.[18] $^1$H and $^{13}$C NMR spectra were recorded on a Bruker US-500 (500 MHz) NMR spectrometer, using $CDCl_3$ or $C_6D_6$ as the solvent unless otherwise noted. Chemical shifts in $^1$H and $^{13}$C NMR spectra are reported in parts per million (ppm, $\delta$ scale). Chemical shifts of $^1$H signals were referenced with TMS (0 ppm) or residual $C_6D_5H$ (7.16 ppm) as standards, and those of $^{13}$C signals were referenced with $CDCl_3$ (77.16 ppm) or $C_6D_6$ (128.06 ppm).[19] The data are presented as follows: chemical shift, multiplicity (s = singlet, d = doublet, t = triplet, q = quartet, m = multiplet and/or multiple resonances, br = broad), coupling constant in hertz (Hz), and integration. Melting points of solid materials were determined on a


DOI: 10.1021/jacs.6b04002
J. Am. Chem. Soc. 2016, 138, 10897–10904

Mel-Temp II capillary melting-point apparatus and are uncorrected. Mass spectra were obtained on a Bruker micrOTOF mass spectrometer. SEM imaging was conducted on an FEI Magellan 400L at a landing voltage of 1 kV under a reduced pressure of $5 \times 10^{-5}$ Pa. AFM observations of PV thin films were carried out on a Bruker Multimode 8 instrument in air.

**General Procedure for Lithium-Induced Reductive Cyclization and Intramolecular Friedel–Crafts Cyclization Reaction.** A Schlenk tube charged with lithium (2.5 equiv relative to compound **8**) and naphthalene (2.5 equiv relative to compound **8**) was evacuated and backfilled with argon three times, then dry THF (0.25 mL per mg of lithium) was added. The tube was sealed under an argon atmosphere and the reaction mixture was stirred at room temperature for 5 h until the lithium was depleted. A Schlenk tube charged with compound **8** was evacuated and backfilled with nitrogen three times, and then dry THF (the same for lithium) was added. The solution of **8** was added to lithium/naphthalene dropwise, and stirred at room temperature for 30 min before the corresponding ketone was added under nitrogen flow. The reaction mixture was stirred at room temperature for another 30 min before being quenched with a few drops of $NH_4Cl$ (aqueous saturated). The crude product was placed on a short column of silica gel with dichloromethane (DCM). After removal of solvents under vacuum, the crude tertiary alcohol was dissolved in carbon tetrachloride (0.4 mL per mg of **8**) without further purification, and boron trifluoride ether complex (2 $\mu$L per mg of **8**) was added. The reaction mixture was stirred at room temperature for 30 min (compounds **9**–**12**) or at 70 °C for 3 h (compound **13**) before being quenched with methanol. After removal of solvents under vacuum, column chromatography over silica gel eluted with hexane/DCM afforded the desired **9**–**13** as white solids.

Compound **9** was prepared following the reported procedure.[15]

*Compound **10** (70% from **8**).* Mp > 250 °C; $^1$H NMR (500 MHz, $CDCl_3$) $\delta$ 7.43–7.45 (m, 1H), 7.33–7.38 (m, 5H), 7.10–7.26 (m, 20H); $^{13}$C NMR (125 MHz, $CDCl_3$) $\delta$ 157.4, 156.0, 142.6, 141.5, 138.4, 137.9, 128.6, 128.5, 127.7, 127.4, 126.4, 126.3, 125.4, 121.4, 120.6, 63.4, 62.3; HRMS (APCI–TOF): calcd for $C_{40}H_{26}Br_2$ 664.0401 ($M^+$), found 664.0422.

*Compound **11** (62% from **8**).* Mp > 250 °C; $^1$H NMR (500 MHz, $CDCl_3$) $\delta$ 7.43–7.45 (m, 1H), 7.35–7.41 (m, 5H), 7.11–7.30 (m, 20H); $^{13}$C NMR (125 MHz, $CDCl_3$) $\delta$ 157.5, 156.3, 156.0, 154.2, 144.6, 142.5, 138.4, 137.8, 131.3, 130.6, 130.3, 128.7, 128.5, 127.8, 127.5, 127.2, 127.1, 126.4, 125.4, 122.9, 121.4, 120.7, 63.4, 62.6; HRMS (APCI–TOF) calcd for $C_{40}H_{26}Br_2$ 664.0401 ($M^+$), found 664.0414.

Compound **12** was precipitated from carbon tetrachloride and washed with methanol to give the product with satisfactory purity as a white solid (78% from **8**). $^1$H NMR (500 MHz, $CDCl_3$) $\delta$ 7.42–7.43 (m, 2H), 7.29–7.31 (m, 8H), 7.22–7.25 (m, 12H), 7.17–7.19 (m, 2H), 7.09–7.15 (m, 4H).

*Compound **13** (73% from **8**).* Mp > 250 °C; $^1$H NMR (500 MHz, $CDCl_3$) $\delta$ 7.73 (d, 2H, $J$ = 8.5 Hz), 7.53 (dd, 2H, $J$ = 8.5, 1.8 Hz), 7.44 (d, 1H, $J$ = 7.5 Hz), 7.39–7.41 (m, 4H), 7.28–7.36 (m, 7H), 7.20 (td, 1H, $J$ = 7.5, 1.0 Hz), 7.08 (td, 1H, $J$ = 7.8, 1.2 Hz), 7.00 (td, 1H, $J$ = 7.5, 1.0 Hz), 6.96 (td, 1H, $J$ = 7.2, 0.8 Hz), 6.91 (d, 2H, $J$ = 1.5 Hz), 6.69 (d, 1H, $J$ = 7.0 Hz), 6.27 (d, 1H, $J$ = 7.5 Hz); HRMS (APCI–TOF) calcd for $C_{40}H_{24}Br_2$ 662.0245 ($M^+$), found 662.0246.

**General Procedure for Bromination with $CuBr_2/Al_2O_3$.** A solution of compounds **9**–**13** in carbon tetrachloride (50 mL/g) was added to $CuBr_2/Al_2O_3$ (3 equiv per reaction site). The reaction mixture was heated at reflux and monitored by TLC. After cooling to room temperature, the reaction mixture was filtered through a plug of silica gel. The solvents were removed under vacuum and the residual was subjected to column chromatography on silica gel eluted with hexane/DCM to afford compounds **14**–**18** as white solids.

Compound **14** was prepared following the reported procedure.[15]

*Compound **15** (99%).* Mp > 250 °C; $^1$H NMR (500 MHz, $CDCl_3$) $\delta$ 7.55 (d, 1H, $J$ = 1.5 Hz), 7.45 (d, 1H, $J$ = 1.5 Hz), 7.40 (d, 4H, $J$ = 9.0 Hz), 7.20–7.30 (m, 12H), 7.09 (d, 4H, $J$ = 8.5 Hz), 7.03 (d, 1H, $J$ = 8.0 Hz), 6.94 (d, 1H, $J$ = 8.0 Hz); $^{13}$C NMR (125 MHz, $CDCl_3$) $\delta$ 159.2, 158.3, 155.4, 153.8, 141.5, 140.4, 137.0, 136.5, 132.1, 131.0, 130.7, 129.9, 128.9, 128.3, 127.7, 122.4, 121.9, 121.7, 120.8, 120.6, 63.5, 62.4; HRMS (APCI–TOF) calcd for $C_{40}H_{24}Br_4$ 819.8612 ($M^+$), found 819.8599.

*Compound **16** (96%).* Mp > 250 °C; $^1$H NMR (500 MHz, $CDCl_3$) $\delta$ 7.55 (d, 1H, $J$ = 1.5 Hz), 7.46 (d, 1H, $J$ = 1.5 Hz), 7.13–7.43 (m, 20H), 7.03 (d, 1H, $J$ = 8.0 Hz), 6.96 (d, 1H, $J$ = 8.5 Hz); $^{13}$C NMR (125 MHz, $CDCl_3$) $\delta$ 159.3, 157.8, 155.7, 153.6, 143.4, 141.4, 136.9, 136.4, 131.2, 131.0, 130.8, 130.5, 129.0, 128.9, 127.7, 126.9, 123.2, 122.4, 121.7, 120.8, 120.7, 63.5, 62.6; HRMS (APCI–TOF) calcd for $C_{40}H_{24}Br_4$ 819.8612 ($M^+$), found 819.8608.

*Compound **17** (95%).* Mp > 250 °C; $^1$H NMR (500 MHz, $CDCl_3$) $\delta$ 7.73 (d, 2H, $J$ = 8.0 Hz), 7.54–7.56 (m, 3H), 7.31–7.38 (m, 11H), 7.12 (d, 1H, $J$ = 8.0 Hz), 7.09 (dd, 1H, $J$ = 8.0, 1.5 Hz), 6.89 (d, 2H, $J$ = 1.5 Hz), 6.80 (d, 1H, $J$ = 2.0 Hz), 6.11 (d, 1H, $J$ = 8.0 Hz); $^{13}$C NMR (125 MHz, $CDCl_3$) $\delta$ 158.7, 153.7, 150.3, 146.0, 141.6, 140.0, 138.4, 135.7, 132.0, 131.4, 130.8, 129.0, 128.7, 128.2, 127.8, 127.1, 126.9, 122.3, 122.2, 122.0, 120.8, 120.6, 120.5, 64.2, 62.2; HRMS (APCI–TOF) calcd for $C_{40}H_{22}Br_4$ 817.8455 ($M^+$), found 817.8438.

*Compound **18** (92%).* Mp > 250 °C; $^1$H NMR (500 MHz, $CDCl_3$) $\delta$ 7.53 (d, 2H, $J$ = 1.5 Hz), 7.23–7.28 (m, 22H), 7.01 (d, 2H, $J$ = 8.0 Hz); $^{13}$C NMR (125 MHz, $CDCl_3$) $\delta$ 159.3, 154.9, 141.7, 137.2, 130.6, 128.8, 128.6, 128.4, 127.5, 122.1, 120.4, 63.4; HRMS (APCI–TOF) calcd for $C_{40}H_{26}Br_2$ 664.0401 ($M^+$), found 664.0381.

Compound **19** was prepared from 2,7-dibromo-9*H*-fluorene following the reported procedure.[20]

**General Procedure for the Buchwald–Hartwig Amination.** A Schlenk tube, charged with the corresponding substrate bromide (**14**–**19**), bis(4-methoxyphenyl)amine (1.5 equiv to C–Br bond), KO*t*-Bu (1.2 equiv to amine), $Pd(dba)_2$ or $Pd_2(dba)_3$ (5% mol Pd per C–Br bond), and *t*-$Bu_3P{\cdot}HBF_4$ (2 equiv to Pd), was evacuated and backfilled with nitrogen three times and dry toluene (25 mL per g substrate bromide). The reaction mixture was stirred at 40 °C for 30 min and then heated at reflux for 48 h before cooling to room temperature. After removal of solvent under vacuum, the residual was flowed through a short column of silica gel with hexane/DCM (plus 1% triethylamine). Preparative gel permeation chromatography (Tol, refraction index detector) gave the product.

*Compound **1** (yellow solid, 94%).* Mp = 173–177 °C; $^1$H NMR (500 MHz, $C_6D_6$) $\delta$ 7.68 (d, 1H, $J$ = 2.0 Hz), 7.60 (d, 1H, $J$ = 2.0 Hz), 7.48–7.50 (m, 4H), 7.44 (d, 4H, $J$ = 9.0 Hz), 7.34 (d, 1H, $J$ = 8.0 Hz), 7.19 (d, 1H, $J$ = 8.5 Hz), 6.86–7.02 (m, 28H), 6.63–6.69 (m, 16H), 3.31 (s, 12H), 3.28 (s, 6H), 3.27 (s, 6H); $^{13}$C NMR (125 MHz, $C_6D_6$) $\delta$ 159.9, 159.0, 156.5, 156.2, 156.1, 154.6, 153.6, 148.0, 147.32, 147.25, 144.3, 141.8, 141.5, 135.6, 133.2, 132.7, 129.8, 129.1, 128.7, 127.3, 127.0, 126.6, 126.5, 121.4, 121.1, 120.8, 120.5, 120.3, 119.9, 119.8, 115.1, 115.0, 63.8, 62.5, 55.04, 55.00; HRMS (APCI–TOF) calcd for $C_{96}H_{81}N_4O_8$ 1417.6054 (M + $H^+$), found 1417.6069.

*Compound **2** (yellow solid, 70%).* Mp = 214–217 °C; $^1$H NMR (500 MHz, $C_6D_6$) $\delta$ 7.60 (d, 1H, $J$ = 2.5 Hz), 7.50 (d, 1H, $J$ = 2.0 Hz), 7.42–7.43 (m, 2H), 7.34–7.36 (m, 4H), 7.13–7.17 (m, 2H), 7.06–7.08 (m, 4H), 6.86–7.01 (m, 25H), 6.76 (dd, 1H, $J$ = 8.2, 2.2 Hz), 6.65–6.72 (m, 16H), 3.31 (s, 12H), 3.284 (s, 6H), 3.278 (s, 6H); $^{13}$C NMR (125 MHz, $C_6D_6$) $\delta$ 158.9, 158.5, 156.3, 156.2, 156.1, 154.0, 153.9, 149.1, 147.1, 144.8, 144.1, 141.9, 141.8, 141.4, 132.6, 132.4, 129.3, 129.0, 128.7, 126.9, 126.8, 126.4, 121.8, 121.5, 121.3, 121.0, 120.9, 120.1, 120.0, 119.5, 119.0, 115.0, 63.9, 63.6, 55.1, 55.0; HRMS (APCI–TOF) calcd for $C_{96}H_{81}N_4O_8$ 1417.6054 (M + $H^+$), found 1417.6101.

*Compound **3** (yellow solid, 95%).* Mp = 162–167 °C; $^1$H NMR (500 MHz, $C_6D_6$) $\delta$ 7.54 (d, 1H, $J$ = 2.0 Hz), 7.37–7.41 (m, 6H), 6.99–7.12 (m, 20H), 6.94 (d, 4H, $J$ = 8.5 Hz), 6.83 (d, 4H, $J$ = 9.0 Hz), 6.67–6.74 (m, 13H), 6.58–6.61 (m, 5H), 6.53 (d, 1H, $J$ = 8.5 Hz); $^{13}$C NMR (125 MHz, $C_6D_6$) $\delta$ 159.3, 157.2, 156.2, 156.0, 155.9, 155.7, 151.4, 148.3, 147.4, 147.3, 143.9, 141.9, 141.7, 136.0, 134.2, 132.0, 128.8, 127.0, 126.4, 126.1, 122.2, 121.7, 121.0, 120.6, 120.5, 119.8, 119.6, 118.5, 117.7, 115.01, 114.97, 144.8, 64.1, 63.1, 55.1, 55.0, 54.9; HRMS (APCI–TOF) calcd for $C_{96}H_{79}N_4O_8$ 1415.5898 (M + $H^+$), found 1415.5902.

*Compound **4** (yellow solid, 71%).* Mp = 183–187 °C; $^1$H NMR (500 MHz, $C_6D_6$) $\delta$ 7.65 (d, 1H, $J$ = 2.0 Hz), 7.58 (d, 1H, $J$ = 2.0 Hz),


DOI: 10.1021/jacs.6b04002
J. Am. Chem. Soc. 2016, 138, 10897–10904

7.50−7.54 (m, 8H), 7.30 (d, 1H, $J$ = 8.5 Hz), 7.20 (d, 1H, $J$ = 8.5 Hz), 6.64−7.06 (m, 20H), 6.61−6.65 (m, 8H), 3.28 (s, 6H), 3.26 (s, 6H), 2.44 (t, 4H, $J$ = 7.8 Hz), 1.46−1.49 (m, 4H), 1.20−1.30 (m, 20H), 0.90 (t, 6H, $J$ = 7.2 Hz); $^{13}$C NMR (125 MHz, $C_6D_6$) $\delta$ 159.4, 159.0, 156.2, 154.4, 153.7, 147.37, 147.33, 144.2, 141.80, 141.77, 141.55, 141.48, 132.9, 132.7, 129.14, 129.10, 128.8, 128.7, 127.0, 126.5, 121.3, 121.1, 120.7, 120.6, 119.8, 115.0, 63.8, 63.3, 55.0, 36.0, 32.3, 31.8, 29.91, 29.89, 29.7, 23.1, 14.4; HRMS (APCI−TOF) calcd for $C_{84}H_{87}N_2O_4$ 1187.6666 (M + H$^+$), found 1187.6656.

*Compound* ***5*** *(yellow solid, 91%).* Mp = 283−284 °C; $^1$H NMR (500 MHz, $C_6D_6$) $\delta$ 7.62 (s, 2H), 7.48 (d, $J$ = 7.0 Hz, 8H), 7.18 (d, $J$ = 8.0 Hz, 2H), 7.02 (d, $J$ = 7.0 Hz, 12H), 6.96 (d, $J$ = 8.5 Hz, 8H), 6.87 (d, $J$ = 8.0 Hz, 2H), 6.71 (d, $J$ = 8.5 Hz, 8H), 3.58 (t, 7.5 Hz, 8H), 1.58 (quint, $J$ = 7.5 Hz, 8H), 1.31 (quint, $J$ = 7.5 Hz, 8H), 1.15−1.25 (m, 16H), 0.86 (t, $J$ = 7.0 Hz, 12H); $^{13}$C NMR (125 MHz, $C_6D_6$); $\delta$ 158.9, 155.8, 153.7, 147.4, 144.0, 141.6, 132.5, 129.1, 128.7, 127.0, 126.5, 121.1, 120.5, 119.6, 115.5, 68.0, 63.7, 31.9, 29.6, 26.1, 23.0, 14.2; TOF MS (APCI$^+$) 1243.7 [M]$^+$; HRMS (APCI$^+$) calcd for $C_{88}H_{94}N_2O_4$ (M) 1242.7208, found 1242.7226.

*Compound* ***6*** *(yellow solid).* Mp = 163−164 °C; $^1$H NMR (400 MHz, $C_6D_6$) $\delta$ 7.44 (s, 2H), 7.22 (d, $J$ = 9.2 Hz, 8H), 7.15 (s, 4H), 6.83 (d, $J$ = 9.2 Hz, 8H), 3.63 (t, $J$ = 6.4 Hz, 8H), 1.41 (s, 12H), 1.60 (quint, $J$ = 6.4 Hz, 8H), 1.34 (quint, $J$ = 7.8 Hz, 8H), 1.15−1.29 (m, 16H), 0.86 (t, $J$ = 6.9 Hz, 12H); $^{13}$C NMR (125 MHz, $C_6D_6$): $\delta$ 161.2, 156.2, 155.0, 147.4, 142.9, 133.1, 126.8, 122.1, 120.3, 118.2, 116.3, 68.7, 45.7, 32.5, 30.3, 26.7, 25.3, 23.6,14.8; TOF MS (APCI$^+$) 994.7 [M]$^+$; HRMS (APCI$^+$) calcd for $C_{68}H_{86}N_2O_4$ (M) 994.6582, found 994.6578.

*Compound* ***7*** *(white solid, 57%).* Mp = 91−93 °C; $^1$H NMR (500 MHz, $C_6D_6$) $\delta$ 7.43 (d, 2H, $J$ = 8.5 Hz), 7.32 (d, 2H, $J$ = 2.0 Hz), 7.21 (d, 8H, $J$ = 9.0 Hz), 7.14−7.16 (m, 2H), 6.79 (d, 8H, $J$ = 9.0 Hz), 3.33 (s, 12H), 1.72−1.75 (m, 4H), 0.99−1.26 (m, 24H), 0.88 (t, 6H, $J$ = 7.2 Hz); $^{13}$C NMR (125 MHz, $C_6D_6$) $\delta$ 156.2, 152.3, 148.0, 142.3, 135.5, 128.3, 126.4, 121.4, 120.0, 117.2, 115.1, 55.3, 55.0, 40.6, 32.3, 30.6, 29.85, 29.83, 24.6, 23.1, 14.4; HRMS (APCI−TOF) calcd for $C_{57}H_{69}N_2O_4$ 845.5257 (M + H$^+$), found 845.5235.

**UV−Vis and Photoluminescence Spectra Measurement.** The UV−vis spectrum of the perovskite thin films on a PEDOT:PSS surface was recorded using a Jasco V-670 spectrophotometer. Photoluminescence of the PV film on glass was performed using a fluorescence spectrophotometer (HITACHI, F-4500).

**Materials.** Methylammonium iodide (MAI) was prepared following previous reports.[11] In a glovebox ($N_2$ atmosphere), MAI, $PbI_2$ (TCI, 99.999%), and $PbCl_2$ (Aldrich, 99.999%) were dissolved in *N*,*N*-dimethylformamide (DMF, Tokyo Chemical Industry Co., 99.5%).

**X-ray Diffraction Measurements.** The XRD experiment was performed on a Rigaku SmartLab X-ray diffractometer equipped with a scintillation counter. The measurement employed the Cu K$\alpha$ line, focused radiation at 9 kW (45 kV, 200 mA) power using a 0.02° 2$\theta$ step scan from 3.0° to 35° with a scanning speed of 3° min$^{-1}$.

**Evaluation of PV Devices.** Current−voltage sweeps were taken on a Keithley 2400 source measurement unit controlled by a computer. The light source used to determine the PCE was an AM 1.5G solar simulator system (Sumitomo Heavy Industries Advanced Machinery) with an intensity of 100 mW/cm$^2$. The SCs were masked with a metal aperture to define the active area of 4 mm$^2$.

**Preparation of SCs.** A fluorine-doped tin oxide (FTO) layer on a glass substrate was used for this study. Prior to the formation of the buffer layer, the patterned FTO glass was ultrasonically cleaned using a surfactant, rinsed with water and then finally given 3 min UV−ozone treatment. A 45 nm thick electron-transporting layer of $TiO_x$ was deposited by spin-coating (3000 rpm for 30 s) of the precursor solution (see materials section) and annealed at 500 °C for 30 min in air atmosphere.[11] To form the $CH_3NH_3PbI_{3-x}Cl_x$ layer, a 40 wt % precursor solution (4:1:1 mol ratio of $CH_3NH_3I$:$PbI_2$:$PbCl_2$) in DMF was spin-coated onto the $TiO_x$ layer at 500 rpm for 3 s and 4000 rpm for 30 s. Further, it was annealed at 100 °C for 35 min in a nitrogen-filled glovebox. The HTL (see materials section) 60 mg/mL in chlorobenzene with dopants (15 $\mu$L, 520 mg/mL Li-TFSI in $CH_3CN$ and 22.5 $\mu$L TBP) was then deposited by spin-coating (2200 rpm for 30 s). The top electrode (Au, 80 nm) was deposited through a metal shadow mask, which defined a 2 mm stripe pattern perpendicular to the ITO stripe.

## ■ ASSOCIATED CONTENT

### Supporting Information

The Supporting Information is available free of charge on the ACS Publications website at DOI: 10.1021/jacs.6b04002.

Photophysical and electrochemical measurements; DFT calculations; energy levels, film XRD, UV−vis spectra, morphology analysis, and $J$−$V$ characteristics of HTLs; and NMR spectra, including Figures S1−S13 and Tables S1−S8 (PDF)

## ■ AUTHOR INFORMATION


### Corresponding Authors

*guoyunlong@chem.s.u-tokyo.ac.jp
*tsujiha@kanagawa-u.ac.jp
*nakamura@chem.s.u-tokyo.ac.jp

### Present Addresses

†Q.Y.: School of Chemistry and Molecular Engineering, East China University of Science and Technology, Meilong Road 130, Shanghai 200237, China
‡H.T.: Faculty of Science, Kanagawa University, 2946 Tsuchiya, Hiratsuka, Kanagawa 259-1293, Japan


### Notes

The authors declare no competing financial interest.

## ■ ACKNOWLEDGMENTS

We thank MEXT for financial support [KAKENHI 15H05754 to E.N., the Strategic Promotion of Innovative Research, JST to Y.G.; Q.Y. is grateful to the JSPS Postdoctoral Fellowship for Foreign Researchers (no. P13334)]. We thank Dr. Nai-Ti Lin for synthesis of compound **6**.

## ■ REFERENCES


(1) (a) Burrezo, P. M.; Zhu, X.; Zhu, S.-F.; Yan, Q.; Lopez Navarrete, J. T.; Tsuji, H.; Nakamura, E.; Casado, J. *J. Am. Chem. Soc.* **2015**, *137*, 3834−3843. (b) Zhu, X.; Tsuji, H.; Lopez Navarrete, J. T.; Casado, J.; Nakamura, E. *J. Am. Chem. Soc.* **2012**, *134*, 19254.

(2) (a) Roldán-Carmona, C.; Malinkiewicz, O.; Betancur, R.; Longo, G.; Momblona, C.; Jaramillo, F.; Camacho, L.; Bolink, H. J. *Energy Environ. Sci.* **2014**, *7*, 2968. (b) Guo, Y.; Shoyama, K.; Sato, W.; Nakamura, E. *Adv. Energy Mater.* **2016**, *6*, 1502317.

(3) (a) Kojima, A.; Teshima, K.; Shirai, Y.; Miyasaka, T. *J. Am. Chem. Soc.* **2009**, *131*, 6050. (b) Nishimura, H.; Ishida, N.; Shimazaki, A.; Wakamiya, A.; Saeki, A.; Scott, L. T.; Murata, Y. *J. Am. Chem. Soc.* **2015**, *137*, 15656−15659. (c) Grätzel, M. *Nat. Mater.* **2014**, *13*, 838. (d) Green, M. A.; Ho-Baillie, A.; Snaith, H. J. *Nat. Photonics* **2014**, *8*, 506. (e) Yin, W.-J.; Yang, J.-H.; Kang, J.; Yan, Y.; Wei, S.-H. *J. Mater. Chem. A* **2015**, *3*, 8926.

(4) (a) Matsuo, Y.; Sato, Y.; Niinomi, T.; Soga, I.; Tanaka, H.; Nakamura, E. *J. Am. Chem. Soc.* **2009**, *131*, 16048−16050. (b) Cf. http://www.japantimes.co.jp/news/2016/02/07/business/tech/technology-improves-future-organic-solar-cells-looks-bright/#.V5rudo787yc.

(5) (a) Burschka, J.; Pellet, N.; Moon, S. J.; Humphry-Baker, R.; Gao, P.; Nazeeruddin, M. K.; Grätzel, M. *Nature* **2013**, *499*, 316. (b) Liu, M.; Johnston, M. B.; Snaith, H. J. *Nature* **2013**, *501*, 395.

(6) Zhu, X.; Tsuji, H.; Yella, A.; Chauvin, A.-S.; Grätzel, M.; Nakamura, E. *Chem. Commun.* **2013**, *49*, 582.

(7) Morales-Vidal, M.; Boj, P. G.; Villalvilla, J. M.; Quintana, J. A.; Yan, Q.; Lin, N.-T.; Zhu, X.; Ruangsupapichat, N.; Casado, J.; Tsuji, H.; Nakamura, E.; Díaz-García, M. A. *Nat. Commun.* **2015**, *6*, 8458.




DOI: 10.1021/jacs.6b04002
J. Am. Chem. Soc. 2016, 138, 10897−10904

(8) Sukegawa, J.; Schubert, C.; Zhu, X.; Tsuji, H.; Guldi, D. M.; Nakamura, E. *Nat. Chem.* **2014**, *6*, 899.
(9) Sukegawa, J.; Tsuji, H.; Nakamura, E. *Chem. Lett.* **2014**, *43*, 699.
(10) (a) Nelsen, S. F.; Ismagilov, R. F.; Powell, D. R. *J. Am. Chem. Soc.* **1996**, *118*, 6313. (b) We thank a reviewer for this interpretation of the ESR spectra..
(11) (a) Guo, Y.; Liu, C.; Inoue, K.; Harano, H.; Tanaka, H.; Nakamura, E. *J. Mater. Chem. A* **2014**, *2*, 13827. (b) Guo, Y.; Liu, C.; Tanaka, H.; Nakamura, E. *J. Phys. Chem. Lett.* **2015**, *6*, 535. (c) Krishna, A.; Sabba, D.; Li, H.; Yin, J.; Boix, P. P.; Soci, C.; Mhaisalkar, S. G.; Grimsdale, A. C. *Chem. Sci.* **2014**, *5*, 2702. (d) Gratia, P.; Magomedov, A.; Malinauskas, T.; Daskeviciene, M.; Abate, A.; Ahmad, S.; Grätzel, M.; Getautis, V.; Nazeeruddin, M. K. *Angew. Chem., Int. Ed.* **2015**, *54*, 11409. (e) Li, M. H.; Hsu, C. W.; Shen, P. S.; Cheng, H. M.; Chi, Y.; Chen, P.; Guo, T. F. *Chem. Commun.* **2015**, *51*, 15518. (f) Park, S.; Heo, J. H.; Cheon, C. H.; Kim, H.; Im, S. H.; Son, H. J. *J. Mater. Chem. A* **2015**, *3*, 24215. (g) Liu, Y.; Hong, Z.; Chen, Q.; Chen, H.; Chang, W. H.; Yang, Y.; Song, T. B.; Yang, Y. *Adv. Mater.* **2016**, *28*, 440. (h) Rakstys, K.; Saliba, M.; Gao, P.; Gratia, P.; Kamarauskas, E.; Paek, S.; Jankauskas, V.; Nazeeruddin, M. K. *Angew. Chem., Int. Ed.* **2016**, *55*, 7464.
(12) Saragi, T. P. I.; Spehr, T.; Siebert, A.; Fuhrmann-Lieker, T.; Salbeck, J. *Chem. Rev.* **2007**, *107*, 1011.
(13) Guo, Y.; Shoyama, K.; Sato, W.; Matsuo, Y.; Inoue, K.; Harano, K.; Liu, C.; Tanaka, H.; Nakamura, E. *J. Am. Chem. Soc.* **2015**, *137*, 15907−15914. Guo, Y.; Sato, W.; Shoyama, K.; Nakamura, E. J. *J. Am. Chem. Soc.* **2016**, *138*, 5410−5416.
(14) Still, W. C.; Kahn, M.; Mitra, A. *J. Org. Chem.* **1978**, *43*, 2923.
(15) Zhu, X.; Tsuji, H.; Nakabayashi, K.; Ohkoshi, S.-i.; Nakamura, E. *J. Am. Chem. Soc.* **2011**, *133*, 16342.
(16) Zhang, Y.; Lu, Z.; Desai, A.; Wulff, D. W. *Org. Lett.* **2008**, *10*, 5429.
(17) Mills, N. S.; Tirla, C.; Benish, M. A.; Rakowitz, A. J.; Bebell, L. M.; Hurd, C. M. M.; Bria, A. L. M. *J. Org. Chem.* **2005**, *70*, 10709.
(18) Fulmer, G. R.; Miller, A. J. M.; Sherden, N. H.; Gottlieb, H. E.; Nudelman, A.; Stoltz, B. M.; Bercaw, J. E.; Goldberg, K. I. *Organometallics* **2010**, *29*, 2176.
(19) Kodomari, M.; Satoh, H.; Yoshitomi, S. *J. Org. Chem.* **1988**, *53*, 2093.
(20) Hung, M.-C.; Liao, J.-L.; Chen, S.-A.; Chen, S.-H.; Su, A.-C. *J. Am. Chem. Soc.* **2005**, *127*, 14576.


DOI: 10.1021/jacs.6b04002
*J. Am. Chem. Soc.* 2016, 138, 10897−10904